Review

Diffuse neutrino background from past core collapse supernovae

By Shin'ichiro Ando,*1,*2,†

Nick Ekanger,*3

Shunsaku Horiuchi*2,*3

and Yusuke Koshio*2,*4

(Edited by Katsuhiko SATO, M.J.A.)

Abstract: Core collapse supernovae are among the most powerful explosions in the Universe, which emit thermal neutrinos that carry away most of the gravitational binding energy released. These neutrinos produce a diffuse supernova neutrino background (DSNB), which is one of the largest energy budgets among all radiation backgrounds. Detecting the DSNB is an important goal of modern high-energy astrophysics and particle physics, which provides valuable insights into core collapse modeling, neutrino physics, and cosmic supernova rate history. In this review, the key ingredients of DSNB calculation and what can be learned from future detections, including black hole formation and non-standard neutrino interactions are discussed. Moreover, an overview of the latest updates in neutrino experiments, which could lead to the detection of the DSNB in the next decade, is provided. With the promise of this breakthrough discovery on the horizon, the study of DSNB has great potential to further our understanding of the Universe.

Keywords: supernova, neutrino

1. Introduction

Thirty-five years ago, a supernova exploded in the neighborhood of our Milky Way galaxy. This supernova, SN1987A, which happened in the Large Magellanic Cloud 50 kpc away from the Earth, provided the first detected neutrino signal from beyond the solar system. In total, 11, 8, and 5 neutrino events were detected by Kamiokande-II, ¹⁾ IMB, ²⁾ and Baksan³⁾ detectors, respectively, which enabled intensive discussions on the core collapse mechanisms and neutrino physics. Not only will the next galactic core collapse supernova be a stunning event for neutrino telescopes, as well as various traditional astronomical observatories, and gravitational wave detectors alike, but it also be the first

Even in the unfortunate event that there is not a galactic supernova in the near future, as a result of significant improvements in detector sensitivity, we can detect neutrinos from supernovae at cosmological distances. Within the Hubble volume, the rate of core collapse supernovae is on the order of one per second, which compensates for the reduction of flux from each supernova. Moreover, especially following the gadolinium upgrade of the SK detector, the detection

multimessenger transient in which all three messengers are observed. If this happens at the Galactic Center, this will yield thousands of neutrino events at the current generation of water Cherenkov detectors such as Super-Kamiokande (SK). Other detectors will also detect hundreds of neutrino events, which cover a wide energy range and various flavor species altogether. For instance, IceCube, a Gtonscale neutrino telescope at the South Pole, and its planned successor, IceCube-Gen2, are precisely sensitive to the time evolution of neutrino luminosity but cannot measure the energy of individual neutrinos. Nevertheless, since the supernova rate is estimated to be few per century, 4) the probability of having such an event over the coming decade is unfortunately small, that is, approximately 10%-30%.

^{*1} GRAPPA Institute, University of Amsterdam, Amsterdam, The Netherlands.

^{*2} Kavli Institute for the Physics and Mathematics of the Universe (WPI), The University of Tokyo, Kashiwa, Chiba, Japan.

^{*3} Center for Neutrino Physics, Department of Physics, Virginia Tech, Blacksburg, Virginia, U.S.A.

 $^{^{\}ast 4}$ $\,$ Department of Physics, Okayama University, Okayama, Japan.

[†] Correspondence should be addressed to: S. Ando, GRAPPA Institute, University of Amsterdam, 1098 XH Amsterdam, The Netherlands (e-mail: s.ando@uva.nl).

of this diffuse supernova neutrino background (DSNB) seems imminent. It is possible to explore various important aspects of the physics of core collapse supernovae and neutrinos by measuring the DSNB spectrum. For instance, the DSNB spectrum will contain information on the cosmic history of supernova rate evolution, neutrino generation mechanism, and the fraction of black holes that form due to the core collapse (in which case, there may not be a supernova associated with it). It also provides an ideal setup for the longest baseline low-energy neutrino experiments to test various new interactions in the neutrino sector with unprecedented sensitivity. To predict the flux of the DSNB spectrum, all these physics ingredients are combined. Since there is no time or directional information available for measurement, only the energy distribution (i.e., spectrum) can be observed for the DSNB. Therefore, the degree of degeneracy for these model ingredients is high. To enable detailed interpretations, one must have sufficient statistics and the most accurate theoretical models as well. The former can be achieved using large-volume neutrino telescopes. A prime example is the SK experiment based in Japan, which recently restarted taking neutrino data with gadolinium to substantially reduce the backgrounds. The latter relies on progress in supernova physics mainly driven by numerical simulations of the core collapse process and neutrino physics that progressed substantially over the previous decades, especially for the oscillation parameters, as well as astronomical observables of supernova and associated quantities.

The studies of the DSNB are reviewed in this article by going over the latest progress in the field. Over the years, predictions exhibited steady improvement⁵⁾⁻⁴¹⁾ and have been the focus in several past reviews⁴²⁾⁻⁴⁴⁾ as well as reviews focusing on particular aspects of the DSNB.⁴⁵⁾ To study supernova and neutrino physics, the state-of-the-art of the SK detector and its sensitivity are also covered.

2. Formalism

2.1. Brightness of the extragalactic neutrino sky. We begin with a simple order of magnitude

sky. We begin with a simple order of magnitude estimate before deriving the rigorous formula with which one can compute the DSNB flux. Each core collapse supernova releases 99% of its gravitational binding energy on the order of $E_b = 3GM_{\rm NS}^2/$

 $(5R_{\rm NS}) = 3 \times 10^{53} \, {\rm erg}$ in the form of thermal neutrinos. Here, $M_{\rm NS}=1.4M_{\odot}$ and $R_{\rm NS}=10\,{\rm km}$ are the mass and radius of a newly born neutron star, respectively. The supernova rate in the Milky Way is estimated to be $\sim 0.02 \,\mathrm{yr}^{-1}$. In combination with the local number density of galaxies, which is estimated to be $0.01\,\mathrm{Mpc^{-3}}$, the local supernova rate density is $\rho_{\rm SN} = 2 \times 10^{-4} \, \rm yr^{-1} \, Mpc^{-3}$. Since the beginning of star formation, the Universe has kept injecting supernova neutrinos, and the time scale can be estimated as the Hubble time $t_H \equiv H_0^{-1}$, where H_0 is the Hubble constant. By multiplying the three, the energy density of the DSNB can be obtained as $\epsilon_{\rm DSNB} = E_b \rho_{\rm SN} t_H \approx 3 \times 10^{-14} \, {\rm erg \, cm^{-3}}$. This is likely a conservative estimate because the rate of supernovae is known to be larger in the past by up to an order of magnitude at the redshifts z = 1-2.

The brightest radiation component in the Universe is the cosmic microwave background (CMB)—the radiation from the Big Bang—whose energy density is $\epsilon_{\rm CMB} = 4 \times 10^{-13}\,{\rm erg\,cm^{-3}}$. The second brightest component after the CMB is the extragalactic background light (EBL, *i.e.*, emissions from stars and those reprocessed via dust absorption and re-emission) covering the infrared, optical, and ultraviolet (UV) wavebands, and its energy density is $\epsilon_{\rm EBL} = (2-3) \times 10^{-14}\,{\rm erg\,cm^{-3}}$, whereas other components at different frequencies (X rays, gamma rays, etc.) are much more subdominant by orders of magnitude. Thus, although we have not seen them yet, one of the brightest radiation components in the Universe is composed of the supernova neutrinos.

We can reach the same conclusion with another simple consideration. For each galaxy, its time-averaged luminosity in supernova neutrinos is $L_{\rm DSNB,gal}=E_bR_{\rm SN,gal}=2\times10^{44}\,{\rm erg\,s^{-1}}$, where $R_{\rm SN,gal}=0.02\,{\rm yr^{-1}}$ is the supernova rate per galaxy. On the other hand, the typical luminosity of galaxies (in starlight) is $L_{\star,\rm gal}=10^{10}L_{\odot}=4\times10^{43}\,{\rm erg\,s^{-1}}$. Therefore, if we average over a long time scale (such as Hubble time), then the Milky Way galaxy shines brighter with supernova neutrinos than its optical photons emitted by stars by a factor of a few. This component must therefore be found observationally.

2.2. Kinetic equation. The differential intensity of the neutrino beam I(E, t)—the number of neutrinos received per unit area, unit time, unit energy range, and unit solid angle—is the most relevant quantity for the DSNB. It is related to the number density per unit energy range, n(E), through $I(E) = n(E)/(4\pi)$, where we adopt the natural unit

 $^{^{-1}}$ Supernovae are stochastic events. However, since their frequency of ${\sim}1\,\mathrm{Hz}$ is way higher than that of the DSNB detection, the DSNB events will look isotropic and diffuse.

of $c=\hbar=1$. Owing to the homogeneity and isotropy of the Universe, the differential number density of the neutrinos, n(E), is independent of spatial coordinates but is a function of the neutrino energy E. The current and near future detectors will have no directional sensitivity to enable the study of the DSNB anisotropies, and thus, the differential flux $F(E)=4\pi I(E)=n(E)$ has been employed in the literature.

We aim to understand the time evolution of the differential number density of the DSNB, n(E, t), which we define as a number of the neutrinos per *comoving* volume per unit energy range. It is related to the phase space density f(E, t) through the following:

$$n(E,t) = \frac{E^2}{2\pi^2} f(E,t)a^3(t),$$
 [1]

where a(t) is the scale factor of the Universe, which converts the physical density to the comoving density. The phase space density f(E,t) depends on (E,t) because the distribution is assumed homogeneous and isotropic, and neutrinos are relativistic, $E=|\vec{p}|$.

The evolution of f(E, t) is described by the following kinetic equation:

$$\hat{L}[f(E,t)] = \mathcal{C}[f(E,t)], \qquad [2]$$

where \hat{L} is the Liouville operator and C is the collisional term.

The Liouville operator \hat{L} in generic spacetime is as follows:

$$\hat{L} = p^{\alpha} \frac{\partial}{\partial x^{\alpha}} - \Gamma^{\alpha}_{\beta\gamma} p^{\beta} p^{\gamma} \frac{\partial}{\partial p^{\alpha}}, \qquad [3]$$

where $\Gamma^{\alpha}_{\beta\gamma}$ is the Christoffel symbol.⁴⁶⁾ By applying this to the Friedmann–Robertson–Walker metric, we have

$$\hat{L}[f(E,t)] = E\frac{\partial f}{\partial t} - H(t)E^2\frac{\partial f}{\partial E},$$
 [4]

where $H(t) = \dot{a}(t)/a(t)$ is the Hubble function. Rewriting this in terms of n(E,t), the Liouville operator acting on n(E,t) becomes

$$\hat{L}[n(E,t)] = E \left[\frac{\partial}{\partial t} - H(t)E \frac{\partial}{\partial E} - H(t) \right] n(E,t). \quad [5]$$

The "collisional" term on the right-hand side is then given by the following equation:

$$C[n(E,t)] = R_{SN}(t)E\frac{dN(E)}{dE}, \qquad [6]$$

where $R_{\rm SN}(t)$ is the supernova rate per comoving volume and dN/dE is the neutrino spectrum per each supernova. In summary, the neutrino kinetic equation is as follows:

$$\label{eq:energy} \left[\frac{\partial}{\partial t} - H(t)E\frac{\partial}{\partial E} - H(t)\right] n(E,t) = R_{\rm SN}(t)\frac{dN(E)}{dE}\,.\,[7]$$

2.3. Solution. We largely follow Ref. 47 to solve the kinetic equation. First, instead of (E,t) variables, we adopt (ε,z) , where z is the cosmological redshift and $\varepsilon = E/(1+z)$. Then, the derivative operators ∂_t and ∂_E can be written as $\partial_t = -H(z)[(1+z)\partial_z - \varepsilon\partial_\varepsilon]$ and $\partial_E = (1+z)^{-1}\partial_\varepsilon$. With these new variables, Eq. [7] can be rewritten as follows:

$$-H(z)\frac{\partial}{\partial z}[(1+z)n(\varepsilon,z)] = R_{\rm SN}(z)\frac{dN}{dE}\bigg|_{E=(1+z)\varepsilon}, \quad [8]$$

which can be integrated to obtain

$$n(\varepsilon, z) = \frac{1}{1+z} \int_{z}^{\infty} \frac{dz'}{H(z')} R_{\rm SN}(z') \frac{dN}{dE} \bigg|_{E=(1+z')\varepsilon}. \quad [9]$$

We are interested in the differential flux of the neutrinos at z = 0, and since F(E) = n(E, z = 0), we finally obtain

$$F(E) = \frac{c}{H_0} \int_0^\infty \frac{dz}{\sqrt{\Omega_m (1+z)^3 + \Omega_\Lambda}} R_{\rm SN}(z) \frac{dN}{dE'} \bigg|_{E'=(1+z)E}.$$
[10]

Here, we note that we recovered c explicitly and used the Friedmann equation in the flat expanding Universe, $H(z) = H_0 \sqrt{\Omega_m (1+z)^3 + \Omega_\Lambda}$, which is dominated by matter and the cosmological constant Λ with their density parameters, Ω_m and Ω_Λ , respectively. Throughout this review, we adopt $H_0 = 67.4 \, \mathrm{km \, s^{-1} \, Mpc^{-1}}$, $\Omega_m = 0.315$, and $\Omega_\Lambda = 0.685$, which are compatible with the latest Planck measurements of the cosmological parameters.⁴⁸⁾

3. Theoretical model ingredients

3.1. Cosmic supernova rate density.

3.1.1. Direct measurements. Although supernovae have been directly observed for centuries, systematic observations that allow their volumetric rates to be inferred have been driven more recently by the rise of large surveys. Since supernovae are transient phenomena, their search necessitates multiple scans of the same target(s). There are broadly two survey strategies to search for supernovae: targeted and nontargeted.

In the targeted strategy, a list of targets (e.g., galaxies) is precompiled and surveyed repeatedly over time. Early surveys⁴⁹⁾⁻⁵¹⁾ often adopted this strategy because the number of discovered supernovae can be maximized by targeting large starforming galaxies. Such surveys therefore often report supernova rates per unit galaxy luminosity in a particular band, SNuB = $1 \text{ SN } (100 \text{ yr})^{-1} (10^{10} L_{\odot}^{\text{B}})^{-1}$, where $L^{\rm B}_{\odot}$ is the solar B-band luminosity. To convert this to the *volumetric* rate necessary for the DSNB, one must account for the luminosity density of the Universe at the redshift in question, which must be independently measured, $j_B(z) = (1.03 + 1.76z) \times$ $10^8 L_{\odot}^B \,\mathrm{Mpc}^{-3.51}$ One concern is that targeted surveys would miss bright supernovae in smaller galaxies not included in the target list, even if they are within the flux sensitivity and volume range of the survey. This must be corrected. In the more recent survey by the Lick Observatory Supernova Search (LOSS),^{52)–54)} over 10,000 galaxies were monitored for 11 years, leading to the discovery of the "rate-size relation", where the supernova frequency is not linearly proportional to the size of the host galaxy but as a power law with an index (of 0.4–0.6), whose exact number depends on the supernova type and galaxy Hubble type. Thus, correcting for missing supernovae is far from a simple scaling exercise.

In the nontargeted strategy, patches of the sky are pre-selected and surveyed repeatedly over time. This locates all supernovae only limited by flux, that is, irrespective of the supernova host galaxy. This means the volumetric rate is more readily estimated. To acquire a large sample of supernovae, a large field of view must be surveyed, especially for nearby distances. Most recent surveys have adopted this method. The Rubin Observatory Legacy Survey of Space and Time (LSST), for example, is expected to survey $\sim 20,000~\rm deg^2$, slightly less than half of the sky, with a planned revisit time of $\sim 3~\rm days$ on average per $10,000~\rm deg^2$ with two visits per night. This will result in an increase in orders of magnitude in the number of supernovae discovered. $^{55),56}$

An important systematic consideration that affects both survey strategies is that of dust extinction. Supernova surveys will miss the faintest supernovae due to flux sensitivity limits.⁵⁷⁾ Over a population, the supernova luminosity has some intrinsic distribution, so naturally, some will fall below the survey sensitivity; however, intrinsically luminous supernovae can also appear significantly fainter because of dust extinction. Typically, the supernova luminosity function is constructed using a

volume-limited sample (for example, either obtained independently or using a subset of nearby supernovae within the survey) and employed to infer the missing faint end in larger flux-limited samples. Nevertheless, dust extinction is redshift-dependent and its modeling for supernovae correction has been updated over the last decades. ^{57),58)} As explained later in Section 3.1.3, it has been highlighted that the direct supernova measurements are systematically lower than the birth rates of massive stars. ⁵⁹⁾ This discrepancy between the birth rates and supernova rates can be remedied by such improved dust modeling.

Furthermore, the DSNB is sensitive to the total core collapse rate, irrespective of whether the collapse yields a luminous supernova or not. In this context, direct measurements of supernovae are likely to fall short, considering that the collapse to black holes is expected to yield systematically dimmer, longer, and redder transients, ^{60),61)} which are not efficiently detected by supernova surveys. ^{62)–64)}

3.1.2. Measurements of birth rates. native method to measure the cosmic supernova rate is indirectly from the cosmic birth rate of stars: the mass of the total stars formed per unit time per unit comoving volume at a given redshift z. This strategy works since the lifetimes of massive stars that undergo supernova explosions (heavier than approximately $\sim 8M_{\odot}$ in mass) are less than O(100) Myr, which is short on cosmological timescales. In other words, all massive stars born in a particular redshift range will expend their nuclear fuel and collapse within the same redshift bin, without a cosmologically significant delay (the same cannot be said about thermonuclear supernovae, 65) which can be delayed by billions of years since the birth of their progenitor stars).

The core collapse rate density is then inferred as follows with the assumption of the stellar initial mass function (IMF) $\phi(M)$:

$$R_{\rm CC}(z) = \frac{\int_{8M_{\odot}}^{125M_{\odot}} dM\phi(M)}{\int_{0.1M_{\odot}}^{125M_{\odot}} dMM\phi(M)} R_{\rm SF}(z), \qquad [11]$$

where $R_{\rm SF}$ is the SFRD and the Salpeter mass function $(\phi(M) \propto M^{-2.35})$ has been adopted often in the literature. Here, the stellar mass distribution spans $0.1 M_{\odot}$ to $125 M_{\odot}$, with the supernova progenitor ranging from $8 M_{\odot}$ to $125 M_{\odot}$. In reality, the Salpeter IMF is known to be inaccurate, especially at the low-mass end, but it is still useful as a common way to compare. Various modifications to the

Salpeter IMF exist, among the more frequently used including those by Chabrier⁶⁷⁾ and Kroupa.⁶⁸⁾

The number of massive stars in a galaxy at a given time is employed to infer the cosmic birth rate of stars. This allows one to determine the mean star formation rate (SFR) of stars during the time span that corresponds to the lifetimes of massive stars. However, it is not feasible to observe individual massive stars in distant galaxies. So instead, aggregate galactic observables are employed to estimate the number of massive stars, the so-called "starformation indicators".⁶⁹⁾ For example, massive stars have high surface temperatures and thus typically dominate a galaxy's UV emission (barring emission from nonstellar origins, e.g., active galactic nuclei, AGN). Thus, observations of a galaxy's UV emission can be combined with knowledge of massive stars' UV luminosities to estimate the recent SFR. The conversion to SFR is known as the "calibration factor", and its modeling typically relies on stellar population modeling. In practice, when the SFR is estimated using, for example, the UV indicator, the observed UV luminosity is appropriately dust-corrected and AGN-corrected (when necessary) and then multiplied by the UV calibration factor. A recent collection of SFRD measurements is shown in Fig. 1 (including UV and other measurements), alongside two commonly used functional fits to the data from Yuksel et al. 2008⁷⁰⁾ and Madau and Dickinson 2014.⁷¹⁾ The spread in measurements is a factor of 2-3 in the redshift range of a few relevant for the DSNB.

Calibration factors have been computed for the various star formation indicators but require a great deal of complex physics, which includes challenging problems such as the evolution of massive stars and its dependence on stellar parameters, such as mass, metallicity, and rotation; modeling of stellar atmospheres, the binary fraction and the resulting interactions, the shape of the stellar IMF, and whether star formation is continuous or variable. The status was summarized by Kennicutt in 1998,⁶⁹⁾ which continues to be used for ease of comparison with other estimates but has also been updated for various specific indicators and circumstances.

One of the primary sources of uncertainty stems from the IMF. The physical explanation for this phenomenon lies in the necessity of extrapolation in mass, which is contingent upon the IMF. To be more precise, although the measurement of star formation relies on the population of massive stars, the *total* SFR is dominated by low-mass stars. Uncertainties

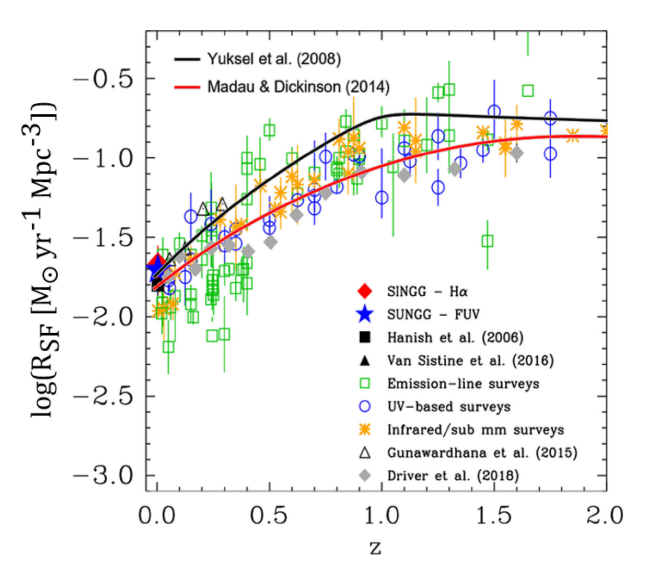


Fig. 1. (Color online) Star formation rate density (SFRD) as a function of redshift. SFRD points collected from the right panel of Fig. 6 of Audcent-Ross *et al.* 2018,⁷² entitled "Near-identical star formation rate densities from $H\alpha$ and FUV at redshift zero", published in Mon. Not. Roy. Astron. Soc. volume 480 no. 1. Fits to other data sets carried out in Madau and Dickinson 2014⁷¹ and Yuksel *et al.* 2008⁷⁰ with Horiuchi *et al.* 2009²¹) parameters are plotted for comparison. All assume the Salpeter IMF.

in the shape of the IMF introduce a factor ~ 2 or more effect on the inferred SFR. Fortunately, this uncertainty does not propagate directly to the DSNB, considering that the DSNB is not powered by low-mass stars. Instead, the DSNB is powered by the same massive stars employed to measure the star formation; hence, the effect of the IMF uncertainty on the supernova rate is at the level of $<10\%.^{21}$) This is also corroborated by a study of the implications of a nonuniversal IMF, where even extreme IMF variations led to small variations in the supernova rate, at least, in the low redshifts of relevance for the DSNB.³⁸)

3.1.3. Core collapse to black holes. As previously stated, the core collapse of a massive star need not necessarily cause a supernova explosion. Indeed, the observation of stellar mass black holes—from microquasars to gravitational waves—provides compelling evidence suggesting that a nonnegligible fraction of massive stars undergo collapse, resulting in the formation of black holes. This phenomenon can potentially lead to potentially lead to no or weak supernova explosions. Nevertheless, these are still powerful neutrino sources.

Thus far, the *in situ* formation of a black hole has not been directly observed. Theoretical investigations suggest the direct collapse of the core of a large red supergiant to a black hole could yield a weak, red, and long-lived transient because of the unbinding of the hydrogen envelope.^{60),61)} Nevertheless, transient surveys are not optimized to detect and record such long and red explosions. Alternatively, if the detection of an explosion proves challenging, the phenomenon of massive stars vanishing could be comparatively more feasible for observation. Such a survey has been in existence for about a decade. This is the "survey about nothing", searching for the disappearance of massive stars without a supernova explosion.⁷³⁾ These stars are then strong candidates for stars that undergo core collapse into black holes. The overarching strategy entails monitoring a sufficient number of massive stars, with the aim of ensuring that, on average, at least one of these stars undergoes core collapse in any given year. Over the course of 11 years, the survey has observed a total of nine massive stars that were shown to be temporally and spatially associated with supernovae and two massive stars disappearing without such coincidence with supernovae. $^{(62),(63),(74)-(76)}$ Naively, this implies a $23.6^{+23.3}_{-15.7}\%$ fraction of massive stars undergoing collapse to a black hole; note that if only one of the disappearing candidates is included, the fraction is $16.2^{+23.2}_{-12.5}\%$. 63) Even for the more conservative latter estimate, it remains a substantially enough fraction to be of interest to the DSNB. Although the uncertainty is large, this is a nonnegligible fraction for the DSNB. One of the benefits of using the SFR is that it does not bias against collapse to black holes.

In principle, precisely knowing the cosmic SFR and the cosmic supernova rate independently can yield the fraction of core collapse to black holes. Early measurements suggested a systematic discrepancy between them, at the factor of ~ 2 level, ⁵⁹⁾ that naively could be interpreted as some half of massive stars collapsing to black holes without luminous supernovae. Nevertheless, there are other factors that might contribute to the faintness of supernovae. with dust extinction being the prominent one (see section 3.1.1). Indeed, the authors 59 found that at nearby distances <20 Mpc, where even dust extinguished supernovae could be more easily detected, the fraction of faint supernovae was much higher than at larger distances, suggesting dust to be an important factor. Since then, updated dust models have been employed for supernova rate measurements, thereby establishing a connection between the supernova rate and SFRs.⁷⁷⁾ Given the existing uncertainties, fractions of $\sim 10-40\%$ appear to be allowed, which is consistent with searches of disappearing stars.

Theoretically predicting the fraction of stars that collapse into black holes is very uncertain at present because of the unknown nature of the explosion mechanism and the need to survey a vast landscape of massive star properties. Attempts have been made assuming the delayed-neutrino heating explosion mechanism and using simpler core collapse simulation treatments to survey large numbers of progenitors. For instance, a recent analysis by the Garching group yields fractions ranging from 17.8% to 41.7%. ³⁶⁾ Consequently, most studies therefore parameterize the fraction of core collapse into black holes.

3.2. Neutrino spectrum from core collapse supernova explosions. Broadly speaking, the following should be considered for DSNB predictions: (i) the emission of neutrinos from the vast range of properties of massive stars in nature; (ii) the time-integrated neutrino emission, often going beyond the time ranges studied by numerical simulations; (iii) the emission of neutrinos from both core collapse to neutron stars and black holes; and (iv) a consideration for neutrino oscillations in the progenitor.

3.2.1. Progenitors. Generally, stars heavier than $\sim 8M_{\odot}$ end their life triggered by a core collapse, leaving a neutron star or a black hole behind. How the core collapse depends on the properties of progenitors such as their mass and rotation has been investigated extensively; nevertheless, it remains far from complete. For example, the conditions for black hole formation after the core collapse were once considered to depend mostly on the mass and metallicity of its progenitor star, with massive and low metals being the important criteria. 78) This implied for galaxies dominated by solar metal stars, the fraction of massive stars collapsing to black holes was small, amounting to only a few percent.⁷⁹⁾ However, it transpired that the situation was more complex than initially anticipated. Shock revival is highly sensitive to the energy transport by neutrinos. This transport is dependent on two factors: the microphysics that governs the emission from the hot-dense core and the three-dimensional turbulence structure that determines the rate of neutrino capture (and hence heating). In other words, the occurrence of an explosion is sensitive to the initial conditions, which appear to be not simply monotonic with, e.g., the stellar mass. $^{36},^{80},^{-83}$ Consequently, the formation of black holes and subsequent failure of supernova can occur even in low-mass progenitors as

light as $\sim 15 M_{\odot}$, whereas very heavy stars can still cause successful explosions.

On the other hand, the neutrino emission can be more accurately characterized. For instance, the stellar compactness parameter, $^{79)}$

$$\xi_M = \frac{M/M_{\odot}}{R(M_{\text{bary}} = M)/1000 \,\text{km}},$$
 [12]

has been discussed in the literature. Here, $R(M_{\text{bary}} =$ M) is a radius enclosing a baryonic mass M. The compactness at $M = 2.5 M_{\odot}$, $\xi_{2.5}$ is a suitable criterion for the black hole formation considering that it is close to the maximal mass of a neutron star,⁷⁹⁾ despite that other masses can provide clearer distinguishing power. $^{82)}$ Horiuchi $\it et~al.^{33)}$ compiled core collapse simulations of $8\text{--}100M_{\odot}$ progenitor masses and found extensive dependence of neutrino emission spectrum on $\xi_{2.5}$. Approximately, a star with higher compactness is characterized by a large massive core, resulting in a prolonged period of intense mass accretion onto the collapsed core. This accretion powers strong neutrino emissions, and thus, both the total energy liberated in neutrinos and the neutrino mean energy grow with compactness. Nevertheless, at some stage, the mass accretion would become too intense and the shock revival cannot be achieved by the neutrinos. This may suggest a critical compactness necessary for collapse into black holes. In reality, this simplistic picture is complicated by several factors, which smears the predictability noticeably. For example, the progenitor density shift at the silicon shell appears to play an essential role in shock revival, 84) which is not sufficiently captured in a simple compactness picture.

Binary effects are another important consideration for supernova progenitors. Observations of stars in the Milky Way and nearby stars reveal that the majority (>50%) of massive stars have experienced binary effects. Binary interactions, especially mass transfer and stellar mergers, can significantly change the masses of core collapse progenitors and strongly influence the DSNB. For instance, stars that are born below the core collapse threshold ($\sim 8M_{\odot}$) may eventually exceed the threshold by, for example, merging with another star. By adopting population synthesis of binary star systems, binary effects were found to enhance the DSNB flux by 15%–20% in favor of future detection. Binary effects

3.2.2. Neutrino emission. Neutrinos are emitted from the surface of the protoneutron star. Therefore, neutrinos—along with gravitational waves—are among the only ways to probe the condition of the

collapsing core. To date, the only observational dataset is the approximately two dozen neutrinos from SN1987A^{1),2)}; thus, to predict the DSNB, we must generally rely on results of numerical simulations of stellar core collapse. They are, however, among the most challenging problems in computational astrophysics, 87)-90) since they involve all the four fundamental forces of nature (electromagnetic, gravitational, strong, and weak forces) that play key roles, and one must address microphysics of neutrino propagation, with gravito-magnetohydrodynamics part of the code. Especially, for obtaining the most realistic outcomes, we should perform the simulations in the three-dimensional setup, including both the coordinate space and neutrino momentum space, which makes it computationally expensive. Nonetheless, researchers from multiple groups have tackled this problem and have obtained reliable results. For instance, they now successfully lead to supernova explosions, especially for low-mass progenitor models. Recent three-dimensional simulations of the $\sim 20 M_{\odot}$ progenitor with elaborate neutrino transfer scheme successfully achieved the explosion energy of $\sim 10^{51}$ erg that matches supernova observations well through neutrino heating mechanism.⁹¹⁾

Despite this notable progress in the core collapse simulations, the majority of simulations remain limited to the initial 1s or so. This is mainly because successful shock revival must occur during the initial second while the neutrino emission is most intense. However, the time-integrated spectrum is relevant for the DSNB flux estimate, and indeed, a substantial fraction of the total neutrino emission is attributed to the later phase of the protoneutron star cooling after 1s (typically >50%). We discuss this deficit in detail in Section 3.2.4.

Multiple independent groups compared one-dimensional results from each of their simulations and confirmed that even with different approximations and so forth, the results are in good agreement. For the neutrino emission, the agreement level is within a few tens of percent. ⁹²⁾ This is also confirmed in Fig. 2, where we compare the time-integrated spectra from five simulation models of a $20\,M_\odot$ progenitor (with the exception of Bollig et~al., ⁸⁸⁾ which is a $27\,M_\odot$ progenitor) up to the first $300\,\mathrm{ms}$ post-core-collapse. ²

 $^{^2}$ All DSNB flux spectra figures are created using our publicly available PyDSNB code, found at https://github.com/shinichiroando/PyDSNB/tree/main. This code makes use of and is consistent with the most recent version of SNEWPY (version 1 3) 93,94

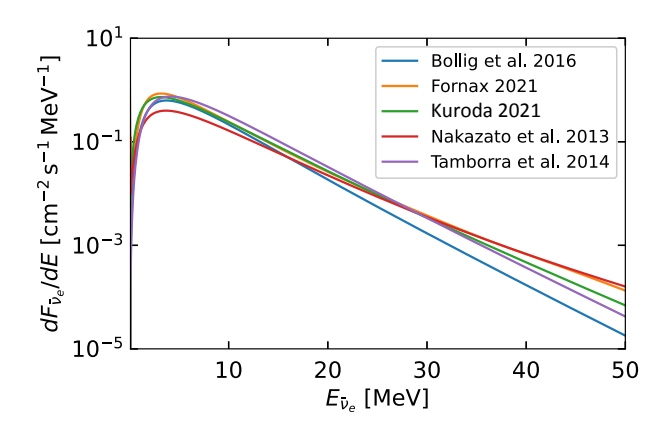


Fig. 2. (Color online) DSNB spectra of different models for the hydrodynamic phase of protoneutron star evolution; each model shown here has been integrated up to the first 300 ms of each simulation for $20\,M_\odot$ progenitors (except for Bollig *et al.* 2016, ⁸⁸) which is a $27\,M_\odot$ progenitor, and the Nakazato *et al.* 2013⁹⁵ model has metallicity Z=0.02). We compare these against the Fornax 2021, ⁹⁰, ⁹⁶ Kuroda 2021, ⁹⁷ and Tamborra *et al.* 2014⁹⁸) models

Since the neutrino spectrum from each core collapse event is dependent on the characteristics of progenitor stars such as their masses, for the estimate of the DSNB flux, one must take the average of dN/dE over mass with the weight of the stellar IMF:

$$\frac{dN}{dE} = \frac{\sum_{i} (dN/dE)_{i} \int_{M_{i}^{i}}^{M_{i}^{u}} dM\phi(M)}{\int dM\phi(M)}.$$
 [13]

Here, one can use a model spectrum $(dN/dE)_i$ in a mass bin i between the lower and upper mass bounds, M_i^l and M_i^u , respectively.

3.2.3. Neutrino oscillations. It is strongly established that the neutrinos have masses and different flavors mix during propagation. These phenomena called neutrino oscillations are well understood in vacuum and matter-dominated environments, particularly because all the mixing angles and mass squared differences have been measured precisely. There remains uncertainty related to the mass hierarchy that can be either normal (NH) or inverted (IH). The MSW mechanism of the matter-induced neutrino oscillations mixes the electron flavors (ν_e and $\bar{\nu}_e$) with heavy-lepton flavors (ν_x collectively representing μ and τ flavor neutrinos and antineutrinos) as follows:

$$F_{\nu_e} = \begin{cases} F_{\nu_x}^0 & \text{(NH),} \\ \sin^2 \theta_{12} F_{\nu_e}^0 + \cos^2 \theta_{12} F_{\nu_x}^0 & \text{(IH),} \end{cases}$$
[14]

for the neutrino sector, and

$$F_{\bar{\nu}_e} = \begin{cases} \cos^2 \theta_{12} F_{\bar{\nu}_e}^0 + \sin^2 \theta_{12} F_{\nu_x}^0 & \text{(NH),} \\ F_{\nu_x}^0 & \text{(IH),} \end{cases}$$
[15]

for the antineutrino sector. Here, θ_{12} is a mixing angle that is relevant for solar and reactor neutrinos $(\sin^2\theta_{12}\approx 0.3^{99})$. For simplicity, we assume $\theta_{13}=0$. Using a more accurate value $(\sin^2\theta_{13}\approx 0.02^{99})$ will have a negligible impact on the obtained results. The superscript 0 represents the flux at production (*i.e.*, before propagation through the stellar envelope and interstellar space).

Around the neutrinosphere where the density of the neutrinos is large, collective oscillations triggered by the neutrino-neutrino interactions can be vital. This is likely to be important in a time-dependent manner, for example, in the next Milky Way core collapse supernova, but could be smeared out in the DSNB spectrum where the signature is integrated over time. 26),34) Nevertheless, the jury is still out given the dearth of predictable collective oscillation patterns. We therefore neglect the effect of collective neutrino oscillation on the DSNB flux and focus only on the MSW effect. Figure 3 shows the DSNB flux spectra for each flavor with a Fermi–Dirac distribution at temperatures of 3.4, 4.1, and 4.1 MeV for ν_e , $\bar{\nu}_e$, and ν_x , respectively, based on the analysis done in Ekanger et al.³⁷⁾ Because the $\bar{\nu}_e$ and ν_x spectra are so similar, the spectrum after MSW oscillation looks very similar for normal and inverted hierarchies.

3.2.4. Late-time evolution. Approximately half of the total neutrinos emitted by a stellar core collapse are during the so-called cooling phase, that is, when

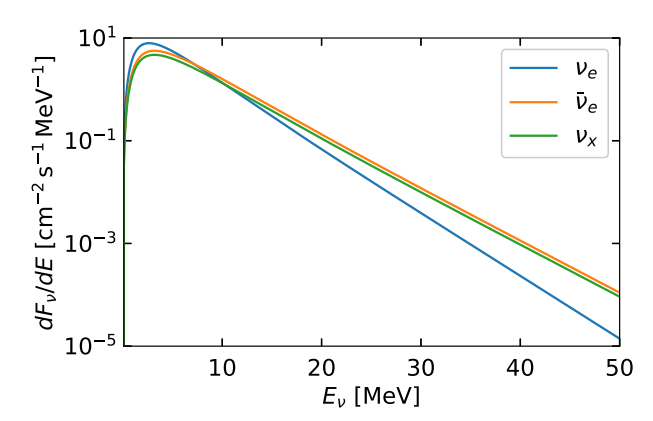


Fig. 3. (Color online) DSNB spectra for the Fermi–Dirac model with parameters derived from the model of Ekanger $et~al.,^{37}$ which have $E_{\nu,e} = 5.8 \times 10^{52} \, \mathrm{erg},~E_{\bar{\nu},e} = 6 \times 10^{52} \, \mathrm{erg},~\mathrm{and}~E_{\nu,x} = 5 \times 10^{52} \, \mathrm{erg},~\mathrm{and}~temperatures~T_{\nu,e} = 3.4 \, \mathrm{MeV}$ and $T_{\bar{\nu}_e} = T_{\nu,x} = 4.1 \, \mathrm{MeV}$. Since $\bar{\nu}_e$ and ν_x have very similar temperatures, the spectrum after oscillation due to the MSW effect looks very similar for normal and inverted hierarchies.

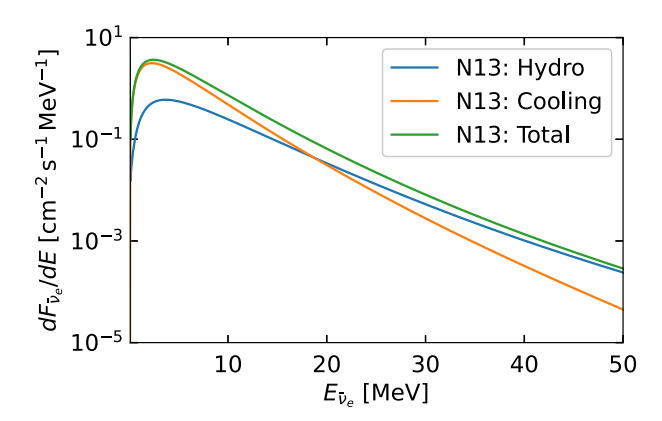


Fig. 4. (Color online) Comparison of the DSNB spectrum from the early hydrodynamic, late cooling, and total phases of the Nakazato et al. 95) (or N13) model. This assumes a revival time of 300 ms, metallicity of Z=0.02, and progenitor mass of $20~M_{\odot}$.

the protoneutron star cools and shrinks by the emission of mostly neutrinos. Simulations dedicated to the cooling phase have been performed, for example, exploring the impacts of the protoneutron star's interior turbulence, the equation of state of hot-dense matter, and other nuclear physics. Nevertheless, due to the considerably different scales from the core collapse phase, it is not easy to simulate the cooling phase in the same code as the core collapse phase. Instead, groups have tied together such simulations in different ways. For example, Nakazato et al. 95) performed an analytic "match" using a userdefined explosion time. Figure 4 shows the DSNB flux spectra for the $20 M_{\odot}$, Z = 0.02, $300 \,\mathrm{ms}$ revival time model from Nakazato et al.⁹⁵⁾ broken into the early hydrodynamical phase, the late cooling phase, and the total spectrum. The later cooling phase is characterized by lower energy neutrinos and contributes significantly to the overall spectrum. Recently, Ekanger et al.³⁷⁾ implemented different schemes to model the cooling phase neutrino emissions on the DSNB and found a factor of ~ 2 difference in DSNB rates between them. Figure 5 shows the differences in flux spectra when estimating the early hydrodynamical phase from Nakazato et al.⁹⁵⁾ and estimating the late phase with four different schemes. Although the estimated neutrino luminosities were different between the schemes implemented, the differences in neutrino energies had a larger impact on the predicted DSNB rates.

3.2.5. Core collapse to black holes. The neutrino emission from a core collapse to a black hole is expected to be systematically different to that from a core collapse to a neutron star. To get an under-

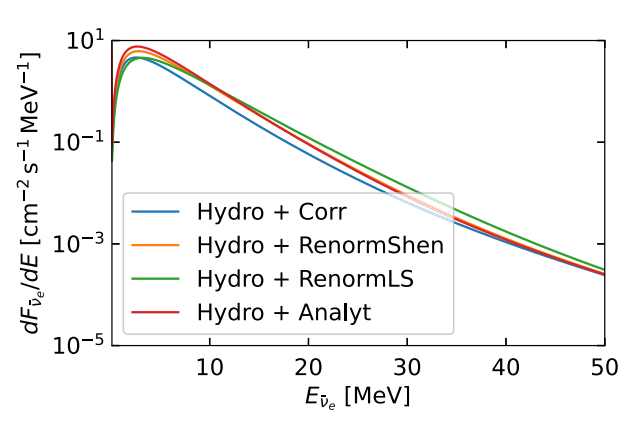


Fig. 5. (Color online) Comparison of the DSNB spectrum of the sum of early hydrodynamic phase plus four different late phase strategies. The data from the hydrodynamic phase is from N13 in this figure, using the same revival time, metallicity, and progenitor mass as Fig. 4.

standing of the matter, it is imperative to acknowledge that the ultimate energy source of neutrinos stems from the gravitational binding energy that is released during the process of stellar core collapses into a more compact object. A collapse to a black hole, which has a larger mass/radius than a neutron star, therefore releases more energy. More energy density equates to higher temperatures and luminosities. In reality, the situation is complicated by the time evolution of the core and the fact that once a black hole is formed, the neutrinos from within the event horizon cannot escape and therefore do not contribute to the total neutrino emission. Consequently, simulations generally find that compared to collapse to neutron stars, collapse to black holes show (i) higher neutrino energies, especially the heavylepton flavor neutrinos whose neutrinospheres are smallest and subject to interior temperatures the most, and (ii) the time-integrated energy released as neutrinos decreases, due to neutrinos not being able to escape. A quicker collapse to a black hole exacerbates these features.³³⁾

The duration of the collapse of a certain core to a black hole is contingent upon both the progenitor and the equation of state of hot-dense matter. For a given equation of state, it is well described by the progenitor's core compactness.^{33),79)} Although the progenitor compactness in large part sets the mass accretion rate and thus the evolution of the mass of the protoneutron star, the equation of state sets the maximum mass of the collapsing central compact object that can be supported. This in turn depends on the stiffness of the equation of state, the amount of

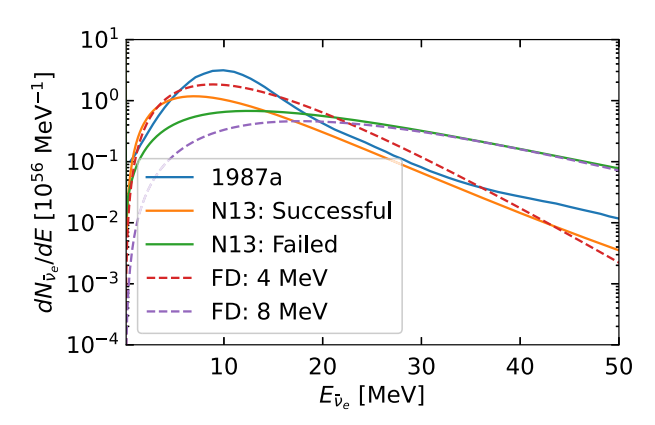


Fig. 6. (Color online) Neutrino number spectrum of successful and failed models of Nakazato $et~al.~({\rm N13})^{95}$) and of SN1987A. (N13) Here, successful N13 model is of $20~M_{\odot}$ progenitor, revival time is $300~{\rm ms}$, metallicity is 0.02, and the equation of state is Shen. (N12) The failed model is $30~M_{\odot}$ progenitor, with 0.004 metallicity, and the equation of state is Shen. Also plotted are Fermi–Dirac distributions for 4 and 8 MeV (3.2 × 10^{53} erg total energy liberated) to represent common estimations of successful and failed supernovae, respectively.

trapped leptons, and the temperature in the accreting protoneutron star. Although various equations of state models have been explored over the years, the addition of more neutron star mass/radii measurements, as well as the discovery of a neutron star merger, has helped to narrow down the range of possibilities. ¹⁰⁰⁾

Figure 6 shows the neutrino spectrum of $\bar{\nu}_e$ flavor for various models of both successful and failed supernovae. We also compare the models with those reconstructed from the SN1987A neutrino data as well as conventional Fermi–Dirac distribution (with zero chemical potential) with the temperature of 4 and 8 MeV. If the core collapse leaves a black hole, then the temperature is higher, which yields the neutrino spectrum close to the Fermi–Dirac distribution with 8-MeV temperature. The core collapse into a neutron star is well approximated as a Fermi–Dirac distribution with 4 MeV temperature.

4. DSNB spectrum

Because of the redshift of neutrino energies, the DSNB flux is dominated by the contribution from supernovae with z < 1 (Fig. 7). At energies above 10 MeV, which is the main target of major detectors, such as Super-K, the DSNB spectrum falls exponentially. Hence, the DSNB spectrum is often plotted with a linear scale for the horizontal axis representing the neutrino energy and with a linear or log scale for the vertical axis representing the flux.

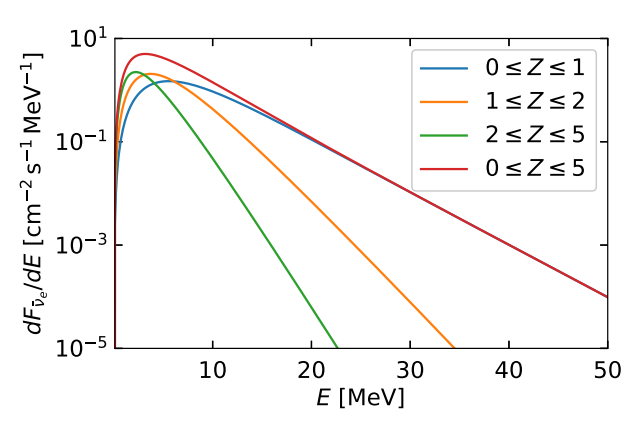


Fig. 7. (Color online) Contributions to the DSNB spectrum from different redshift ranges. The DSNB flux is dominated mostly by supernovae with z < 1. The Fermi–Dirac distribution with $E_{\rm tot} = 3.2 \times 10^{53} \, {\rm erg}$ and $T_{\bar{\nu}_e} = T_{\nu_x} = 4.1 \, {\rm MeV}$ has been adopted.³⁷⁾

With the current detection technology, one can adopt neither time nor spatial information and thus must rely solely on the energy information to probe physics and astrophysics relevant to the DSNB. Yet, with the high statistics expected with the future generation of neutrino detectors, one can extract different important information on the supernova rate, black hole formation, and neutrino physics. We elaborate on each of them in the following:

4.1. Neutrino spectrum of various flavors. Although the dominant detection channel for the DSNB is the inverse beta decay for the $\bar{\nu}_e$ flavor, it is desirable to detect all the flavors $(\nu_e, \bar{\nu}_e, \text{ and } \nu_x)$ to reach a comprehensive understanding of the supernova explosion. We can study $\bar{\nu}_e$ fluxes with Super-K and Hyper-K, whereas a good option for the ν_e flux would be DUNE, which can reach DSNB sensitivity if backgrounds can be controlled. $^{103)}$ The nonelectron flavors ν_x are the hardest to detect, as one must rely on neutral current interactions. These are not efficient at MeV energies because either the crosssection is suppressed (for neutrino-electron scatterings) or the target is too heavy (for neutrino-nucleon scatterings). This challenge can be achieved with existing and future dark matter direct-detection detectors such as XENON, LZ, and DARWIN. Especially with the ultimate dark matter detector, DARWIN, one can reach sensitivity about an order of magnitude larger than theoretical predictions. 104) The neutral-current interaction off the protons in detectors can also be adopted: νp scattering. It has been studied that if the backgrounds against detecting these scattering events could be well understood

and suppressed, one could constrain the ν_x flavor content using JUNO-like detectors. Another suggested opportunity is to use ancient minerals as track detectors, that is, paleo detectors, thick would record supernova neutrinos over geological timescales. Since the relevant interaction for supernova neutrinos is coherent scattering, all flavor information will be obtained, which can be disentangled by a combined analysis with ν_e and $\bar{\nu}_e$ results. However, note that paleo detectors will record more of the historical record of Milky Way supernova neutrinos rather than the DSNB. This means that although still an average over many supernovae, it is not the true DSNB; the traveled baseline and progenitor samples will be different.

4.2. Tests of neutrino physics. Considering that the DSNB can be regarded as the longest baseline (at a cosmological distance scale) low-energy (MeV) neutrino experiment, one can probe unique new physics beyond the standard model in the neutrino sector. Nonradiative neutrino decay induced by the interactions with scalar or pseudo-scalar fields such as Majoron is one such example, where the DSNB can improve upon the sensitivity to neutrino lifetimes by orders of magnitude. 47),108),109) Likewise, one can test the pseudo-Dirac nature of neutrinos as it would yield oscillation between the active and sterile species during propagation, and a unique window in the relevant mass-scale parameter $m_k =$ 10^{-25} – 10^{-24} eV can be tested.¹⁰⁹ If the sterile neutrinos at eV mass scales exist and they interact with a new unknown gauge vector boson ϕ , then such a scenario can be tested using the DSNB. If $M_{\phi} = 5$ 10 keV and the coupling to the sterile neutrinos $g_s = 10^{-4} - 10^{-2}$, it would show a characteristic dip in the DSNB energy spectrum that should be captured by the detectors. 110)

4.3. Cosmology and astrophysics. The DSNB spectrum could also be used to test cosmological models. By using the DSNB data, one can test the standard Λ CDM model including the measurement of the Hubble constant¹⁰⁹⁾ or other exotic models such as a logotropic universe and a bulk viscous matter-dominated universe.¹¹¹⁾

4.4. Core collapse to black holes. As shown in Section 3.2.5, the neutrino spectrum (both the normalization and spectral shape) depends on the final state of the collapsed object—a neutron star or a black hole. One can use the DSNB spectrum to test the black hole formation after the core collapse, which is challenging using optical observations alone. The flux of models with 100% BH formation, with a

few equations of state, $^{39)}$ have already exceeded the 90% confidence level upper limits. $^{112)}$ This means that one can already constrain the fraction of the formation of black holes or high-mass neutron stars. Future observations with SK-Gd and Hyper-K have the potential to significantly constrain the values of these parameters to below tens of percent levels. $^{34)}$

5. Detection prospects

5.1. Detection principle and the history of the observation. There are mainly two types of detectors for DSNB observation. One is the water Cherenkov detector, and the other is the liquid scintillator detector. In a water Cherenkov detector, photodetectors, such as photomultiplier tubes, detect the Cherenkov light produced by charged particles scattered by neutrinos in water. Cherenkov light is emitted when a charged particle traverses a medium at a velocity greater than the speed of light reduced by the refractive index. The Cherenkov light is emitted at an angle to the direction of the charged particle due to the refractive index and its velocity; thus, it is detected as a ring image. If the charged particle is traveling at nearly the speed of light in water, this angle is 42°. In a liquid scintillator detector, the scintillation light generated by the charged particles as they pass through the material is detected using photodetectors. Since the light yield is higher than the water Cherenkov detector, it has a lower energy threshold and higher neutron tagging efficiency after neutrino interactions.

The dominant detection reaction with the largest interaction cross-section in the DSNB energy region is the inverse beta decay (IBD): $\bar{\nu}_e + p \rightarrow e^+ +$ n. The total cross-section is roughly calculated as $\sigma_{\rm tot} \sim 9.52 \times 10^{-44} \ (p_e E_e / {\rm MeV}^2) \, {\rm cm}^2$, and the detailed calculations have been published by several authors. 113),114) In this interaction, positron as a prompt signal is detected, in several detectors, followed by gamma rays from neutron capture on proton or nucleus as a delayed signal. Here, the gamma ray energy depends on what the neutron is captured by, for example, it is 2.2 MeV in the case of proton capture. This detection method is called delayed coincidence (DC) and is effective in the reduction of background events compared to measuring only a prompt signal. In this interaction, the neutrino energy is easily reconstructed from the prompt positron energy using the following equation: $E_{\nu} \sim E_{e^+} + m_n - m_p$, where m_n and m_p are the neutron and proton mass, respectively.

Since the 1980s, DSNB searches have been made with various detectors and, in this section, we briefly introduce each detector and the results. Unfortunately, all experiments have not observed a significant signal of DSNB and only set a 90% C.L. upper limit on it. There are two methods for calculating the limit. One is the so-called 'model-independent search', which is estimated from the number of observed events and the expected background rate without assuming any DSNB or other physics models, which means a flux upper limit of electron antineutrinos. The other is the so-called 'model-dependent search', which is derived by fitting the observed energy spectrum to the spectral shape of the signal from a DSNB model and the background. Here, we will focus on the results of the model-independent search, that is, the electron antineutrino flux upper limit. Additionally, we will comment on the results of the model-dependent search for some detectors.

The first observation of the DSNB was reported by Kamiokande-II in 1988. It was a 2,140-ton water Cherenkov detector in the Kamioka mine, in Japan. It is famous for the first detection of neutrinos from a supernova explosion. For the DSNB observation, the limit of the electron antineutrinos in the energy region between 19 and 35 MeV was set to $226\,\mathrm{cm^{-2}\,s^{-1}}$ by the exposure of $0.58\,\mathrm{kton\cdot year}$.

The next observation was reported by LSD in 1992. The was a liquid scintillation detector, which can tag neutron signals generated via IBD using the DC technique by proton capture. The upper limit of electron antineutrinos with the exposure of 0.0939 kton-year was 9.0×10^4 and $8.2 \times 10^3 \, \mathrm{cm}^{-2} \, \mathrm{s}^{-1}$ for $9 < E_{\nu}/\mathrm{MeV} < 50$ and $20 < E_{\nu}/\mathrm{MeV} < 50$, respectively. They also reported the results of neutrino interactions with carbon nuclei, which are sensitive to other flavors of neutrinos although the cross-sections are approximately one order of magnitude lower, and the energy thresholds are higher than those of IBD.

The situation, that the upper limits are two orders of magnitude higher than the theoretical expectations, has drastically changed since SK began in 1996. It is a 50-kton water Cherenkov detector in the Kamioka mine, in Japan. It is famous for the discovery of neutrino oscillation in atmospheric neutrinos. The first result of the DSNB observation in SK was reported in 2003. In this paper, the first phase of SK was used, and the upper limit of electron antineutrinos above 19.3 MeV was $1.2 \, \mathrm{cm}^{-2} \, \mathrm{s}^{-1}$ by the exposure of $92.2 \, \mathrm{kton} \cdot \mathrm{year}$. The second report appeared in 2012, where the

combined results of phase I through III in SK with the exposure of 176 kton-year using only prompt signals were reported. Figure 8 shows the flux upper limit of electron antineutrinos as a function of neutrino energy. Since the fourth phase of SK (SK-IV) started in 2008, new electronics were installed. 120) It enabled the background events reduced by detecting 2.2 MeV gamma ray from proton capture of a neutron. SK demonstrated successful detection of the neutron capture signal, although the efficiency was low $(\sim 20\%)$. The results using the full data set of SK-IV were reported in 2021.¹¹²⁾ A new analysis method for efficient background reduction and an improved neutron tagging algorithm allowed lowering the energy threshold to 9.3 MeV. The flux upper limit is shown in the figure by the exposure of 183 kton year. Moreover, the combined analysis of all phases of SK was conducted, and the flux limit for electron antineutrinos above 17.3 MeV was set to $2.7\,\mathrm{cm^{-2}\,s^{-1}}$ with the exposure of $359\,\mathrm{kton\cdot year}$. In this paper, a model-dependent search with 21 modern DSNB predictions was also carried out. A 1.5σ level of excess was observed over the background prediction across all the models, and the DSNB flux limits were between 2.5 and $2.8 \,\mathrm{cm}^{-2} \,\mathrm{s}^{-1}$.

Another water Cherenkov detector, Sudbury Neutrino Observatory (SNO), also reported some results of DSNB observations. SNO was located in the Inco, Ltd., Creighton mine near Sudbury, Ontario, Canada, which used ultrapure heavy water. By using heavy water, SNO enabled very unique neutrino observations, which could measure the charged current $(\nu_e + d \rightarrow p + p + e^-)$ and neutral current $(\nu + d \rightarrow \nu + p + n)$ interactions independently. This led to conclusive evidence that neutrino oscillation also occurs in solar neutrinos. (122) As for the DSNB measurements, SNO showed the unique results that were the flux limit of electron neutrinos using the charged current interaction, instead of the electron antineutrinos, which was rather high. $^{123),124)}$ The result in the energy region between 22.9 and 36.9 MeV was 70 cm⁻² s⁻¹ with the exposure of $0.65 \,\mathrm{kton\cdot year}$.

Recently, the results of DSNB observations by two liquid scintillator detectors were shown: One was KamLAND, and the other was Borexino. The KamLAND experiment uses 1 kton of ultrapure liquid scintillator located in Kamioka mine, in Japan. It started in 2002, including KamLAND-Zen, which set the balloon-filled xenon-loaded liquid scintillator at the center in 2011 for the discovery of the neutrinoless double beta decay. For the DSNB

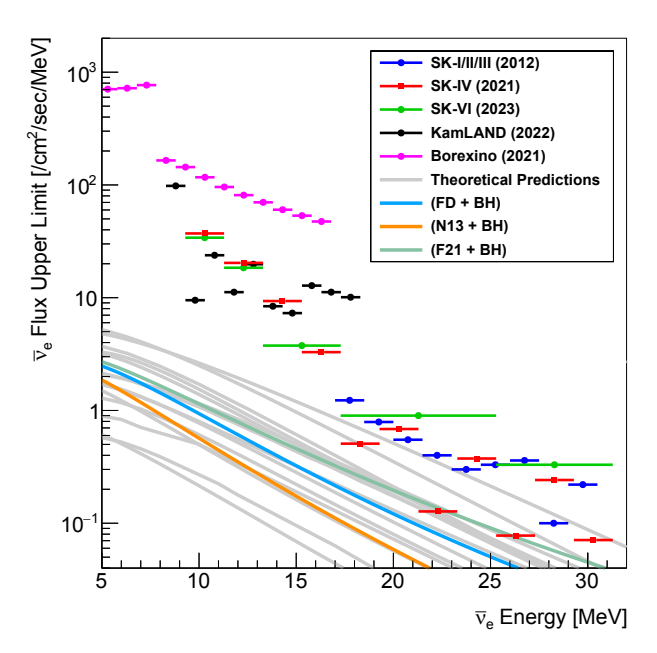


Fig. 8. (Color online) The model-independent upper limits of electron antineutrino flux at 90% C.L. from various recent experiments, SK-I/II/III, 119 SK-IV, 1129 SK-VI, 128) KamLAND, 126) and Borexino in the case including atmospheric neutrino background, 127) overlaid with various DSNB theoretical predictions. Particularly, three models computed as part of this review are shown in color: a Fermi–Dirac distribution withtotal energy 3.2 × 10⁵³ erg and temperature 4.1 MeV (FD+BH), Nakazato et al. 95) IMF-weighed spectrum (N13 + BH), and Fornax (2021) 90),96) IMF-weighed spectrum (F21 + BH). Here, we do not assume a late phase treatment. A Salpeter IMF is used, the black hole fraction is fixed to be 23.6%, and the black hole model is from Nakazato et al. 95) assuming a Shen EOS.

observations, the first results were published in 2012.¹²⁵⁾ followed by the results using more data and improved analysis methods in 2022. 126) In the latest result, the flux upper limit in the energy region between 8.3 and 30.8 MeV with the exposure of 6.72 kton-year was shown in Fig. 8. It gave the most stringent flux limit below 13 MeV, although it was still an order of magnitude larger than DSNB theoretical expectations. The Borexino experiment used 278 tons of ultrapure liquid scintillator located in the underground hall C of Gran Sasso, Italy. Thanks to the exceptionally low level of radiopurity Borexino realized a low-energy threshold. It led to the first discovery of low-energy solar neutrinos such as ⁷Be, pep, pp, and CNO cycle. For the DSNB search, neutrinos in a wide energy range from 1.8 to $16.8\,\mathrm{MeV}$ were searched. $^{127)}$ The flux upper limit with the exposure of 1.494 kton year is shown in the Fig. 8. The flux limit below 8.3 MeV was set only by Borexino.

As described in the 5.2. Backgrounds. previous section, the DSNB has not yet been discovered. It is limited by background events. The DC method is effective for DSNB analysis to search for IBD events, and it has recently become available for water Cherenkov detectors as well as liquid scintillator detectors. Nonetheless, there are still background events that can mimic IBD events. At first, there are two major background sources: One is from spallation products induced by cosmic muons, and the other is from atmospheric neutrinos. They are background events common to the two types of detectors, but there are also differences in the events observed in each type of detector. Additionally, reactor neutrinos can be background events in lower energy regions, and accidental coincidence backgrounds, which mimic DC events, should be considered in both types of detectors. For liquid scintillator detectors, fast neutrons are also one of the backgrounds. In this section, these backgrounds in the DSNB analysis are described.

5.2.1. Spallation products. Cosmic ray muons can penetrate detectors located deep underground, although the rate is drastically reduced relative to sea level. These muons interact with the nuclei in the detector and produce various radioactive isotopes called 'spallation products'. The energies of the spallation products, β and/or γ , are similar to those of positrons from DSNBs. Most of these events can be removed using temporal and spatial correlations with muons. Nevertheless, long-lived products are not easy to remove since it is quite challenging to identify their parent muon and can eventually become background events in DSNB analysis. Particularly, ⁹Li, which undergoes beta decay (35% of which emit one neutron) and has a higher production yield, is one of the remaining background events.

5.2.2. Atmospheric neutrinos. When primary cosmic rays, which are mainly composed of protons, collide with nuclei in the Earth's atmosphere, several hadrons, such as pions and kaons, are generated. Atmospheric neutrinos are generated when these hadrons decay. The energy of atmospheric neutrinos is on the order of 100 MeV to PeV, peaking at several hundred MeV. Particles generated by atmospheric neutrino interactions in the detector have a wide range of energies. If they have reconstructed energy in the DSNB analysis region and neutrons are emitted together, a background event will be constituted. Both charged current (CC) and neutral current (NC) interactions cause such events. Here,

targets of neutrino interaction in the detector are nuclei (oxygen for water, carbon for liquid scintillator) and free protons.

As for the water Cherenkov detector, the most serious background is the neutral current quasielastic interaction, which knocks out a nucleon in oxygen nuclei. If the knocked-out nucleon is a neutron and the excited nucleus generates gamma rays on deexcitation, it is indistinguishable from a DSNB signal because the gamma ray energy is similar to that of the positron in IBD.¹²⁹⁾ Accurate estimation of this background is not easy because of several uncertainties in the nuclear models. Additionally, other interactions, such as an NC interaction with one pion $(\nu + N \rightarrow \nu + N' + \pi)$ or a charged current quasi-elastic interaction (CCQE, $\nu + N \rightarrow l + N'$, where N and N' are nucleons and l is a lepton), could be backgrounds. However, this is the case if neutrons are emitted together.

For liquid scintillator detectors, estimating the background NC interaction with carbon is also challenging due to its uncertainties. The most dominant process is $\nu(\bar{\nu}) + ^{12}C \rightarrow \nu(\bar{\nu}) + n + ^{11}C + \gamma$, but all possible interaction modes are considered in Ref. 125. Compared with that of NC, the contribution of CC is not much. In the case of CC, interaction with free proton is dominant over that with carbon nuclei because of their cross-section. Here, the muon antineutrino interaction is more likely to be the background in the DSNB analysis energy region than electron antineutrinos since a large fraction of the initial neutrino energy is spent to generate muon and the observed energy is shifted to low.

5.2.3. Reactor neutrinos. Reactor neutrinos are produced by the beta decay of neutron-rich fission fragments mainly from the following four isotopes: ²³⁵U, ²³⁸U, ²³⁹Pu, and ²⁴¹Pu. The flux is calculated from reactor operating data such as thermal power generation, fuel burn, shutdown, and fuel reload schedules. The energy spectrum is calculated based on experimental results. ¹³¹⁾ Most reactor neutrinos have energies below 10 MeV, where the DSNB flux is still analyzed.

5.2.4. Accidental coincidence. In actual data acquisition, the prompt signal can be paired with a delayed signal that is misidentified due to a radioactive event or noise, which is called "accidental coincidence". This background event is estimated for each experiment.

5.2.5. Fast neutrons. In a liquid scintillator detector, fast neutrons produced by cosmic muons in the surrounding rock and water and introduced into

the detector can also be background events. Prompt events can be mimicked by the scattering of neutrons on protons or carbon nuclei, followed by a delayed event when the neutron is thermalized and captured on a proton or carbon nucleus.

5.3. Recent upgrade of SK. In the summer of 2020, SK moved to a new phase with the start of SK-Gd, which drastically improved the detection sensitivity of DSNB by adding gadolinium. As described above, neutron tagging in IBD is crucial for background reduction in water Cherenkov detectors. The original idea for this purpose in SK was proposed in 2004.¹³²⁾ Gadolinium has the largest neutron capture cross-section of all elements, giving, for example, a neutron tagging efficiency of 90% at a mass concentration of only 0.1%. Additionally, the delayed gamma ray energy is about 8 MeV in total, which is high enough to be detected by SK. After years of research and development¹³³⁾ and a tank refurbishment work to mainly repair a water leak in 2018, 13 tons of gadolinium sulfate equivalent to 0.011% mass concentration were loaded in 2020¹³⁴ as a first step, and this phase is called SK-VI.

The first result using approximately 1.5 years of data from SK-VI appeared in Ref. 128. This analysis did not assume any spectral shape of the astrophysical electron antineutrino sources as well as the DSNB. Thanks to a significant increase in neutron tagging efficiency (35.6 \pm 2.5%) mainly with gadolinium capture and low misidentification probability $(\sim 10^{-4})$, the IBD signal efficiency was twice that of the previous pure water phase. The events observed in the searched neutrino energy range of 9.3 to 31.3 MeV were consistent with the expected background, mainly due to atmospheric neutrinos and spallation products like ⁹Li. Although no significant signal was discovered from this result, its detection sensitivity was comparable to that of the previous pure water phase, SK-IV, by only one-fifth of statistics. The flux upper limit with 34.0 kton-year in SK-VI is shown in Fig. 8.

In the summer of 2022, an additional 26 tons of gadolinium sulfate were loaded into the detector as a second step. The loading work was successfully completed in about a month. Consequently, gadolinium equivalent to a mass concentration of approximately 0.03% was introduced into SK, and this new experimental phase is called SK-VII. The neutron tagging efficiency was confirmed to be 1.5 times higher than in SK-VI, which was consistent with expectation. In addition to improving neutron tagging efficiency, this phase will allow analysis with

large statistics data assuming the spectral shape of each DSNB model.

5.4. Experiments in the near future.

5.4.1. JUNO. JUNO (Jiangmen Underground Neutrino Observatory) is the next-generation neutrino detector, which is located in Jiangmen in Guangdong province, China. It is the largest liquid scintillator detector ever, with the primary goal of accurately measuring neutrino oscillations from reactor antineutrinos. Moreover, it will be a pioneering experiment to observe the DSNB signal for the first time together with SK-Gd in the next decade. After many years of construction, it will be operational in 2024. The detector is 20 kton of liquid scintillator with 17,612 20-inch and 25,600 3-inch photomultiplier tubes that are installed in the gaps between the 20-inch photomultiplier tubes to enhance the energy resolution. The signal detection method is the same, that is, the DC technique with proton capture via IBD.

Backgrounds for the DSNB search to be considered are described above. First, the $\bar{\nu}_e$ from reactor and atmospheric neutrinos are inevitable. The energy region of reactor neutrinos is less than 10 MeV, whereas the energy region of atmospheric neutrinos increases with the neutrino energy. Thus, the search for DSNB is in the energy region in between. Other backgrounds could be long-lived isotopes due to muon spallation, especially ⁸He and ⁹Li. This is because the β -n decay of these isotopes is very similar to the IBD signal. Nevertheless, the energy of the prompt signal due to the beta decay is relatively low, allowing this background to be ignored if an appropriate energy threshold is set. External fast neutrons could also be a background in liquid scintillator detectors. They are, however, expected to be removed by appropriate fiducial volume cuts. As described above, the estimation and reduction of background due to atmospheric neutrino NC interaction with carbon is challenging. The experimental group has devised various methods to reduce this background and has demonstrated their effectiveness through simulation studies. (135)

5.4.2. Hyper-Kamiokande. Hyper-Kamiokande is the next-generation water Cherenkov detector located 8 km from the SK site. It is now under construction and will start operation in 2027. It is based on a well-established technology with a fiducial volume of 187 ktons, which is 8.3 times larger than that of SK. This huge volume of the detector allows DSNB observations with large statistics as well as other physics targets, thereby promising, for

example, the observation of the DSNB spectrum. The first phase uses pure water; thus, the energy threshold is as high as about 16 MeV due to the effect of the spallation background. Nevertheless, if a DSNB signal with sufficient statistics is observed in the higher energy region, for example, it is sensitive to the black hole formation rate and can provide information on the history of star formation and its metallicity. In the future, if the gadolinium loading is realized, the energy threshold for a DSNB search can be lowered to about 10 MeV. This would make it possible to explore the history of supernova explosions back to an age with a redshift of approximately 1. Thus, Hyper-Kamiokande has the potential to perform neutrino astronomy and cosmology with DSNB observations.

6. Outlook and conclusions

This is an exciting era for neutrino astrophysics. The detection of extraterrestrial neutrinos from an astrophysical origin associated with stellar explosions is just around the corner. DSNB provides valuable information about past core collapse, including the fraction of black hole-forming collapse and neutrino physics through flavor oscillations or other exotic interactions over cosmological baselines. Although detecting the DSNB and studying supernova physics and neutrino properties are challenging goals, recent progress in neutrino experiments makes this an achievable goal in the next decade. For instance, the recent upgrade of the SK detector has significantly reduced background noise, bringing the first detection of DSNB within reach. This review has gathered essential information on DSNB physics and the latest updates from DSNB search experiments. In parallel, we will likely see in the next decades the second detection of neutrinos from a core collapse supernovae after SN1987A that happened more than a quarter century ago. Besides the mere excitement of detection, it will bring plenty of physics and astrophysics to be studied using the rich multimessenger observational data. The coming decades therefore hold great promise for detecting and studying supernova neutrinos, with potential exciting breakthroughs.

Acknowledgments

This work was supported by MEXT KAKENHI Grant Numbers, JP20H05850, JP20H05861 (SA), NSF Grant No. AST-1908960 (NE, SH), No. PHY-2209420 (NE, SH), NSF Grant No. PHY-1914409 (SH), the U.S. Department of Energy Office of

Science under award number DE-SC0020262 (SH), JSPS KAKENHI Grant Number JP22K03630 (SH), JP23H04899 (SH), 20H00162 (YK), and World Premier International Research Center Initiative (WPI), MEXT, Japan (SA, SH, and YK).

References

- Hirata, K., Kajita, T., Koshiba, M., Nakahata, M., Oyama, Y., Sato, N. et al. (1987) Observation of a neutrino burst from the Supernova SN1987A. Phys. Rev. Lett. 58, 1490–1493.
- Bionta, R.M., Blewitt, G., Bratton, C.B., Casper, D., Ciocio, A., Claus, R. et al. (1987) Observation of a neutrino burst in coincidence with supernova 1987A in the Large Magellanic Cloud. Phys. Rev. Lett. 58, 1494.
- Alekseev, E.N., Alekseeva, L.N., Krivosheina, I.V. and Volchenko, V.I. (1988) Detection of the neutrino signal from SN1987A in the LMC using the Inr Baksan Underground Scintillation Telescope. Phys. Lett. B 205, 209–214.
- Rozwadowska, K., Vissani, F. and Cappellaro, E. (2021) On the rate of core collapse supernovae in the milky way. New Astron. 83, 101498.
- Krauss, L.M., Glashow, S.L. and Schramm, D.N. (1984) Anti-neutrinos astronomy and geophysics. Nature 310, 191–198.
- Dar, A. (1985) Has a cosmological neutrino background from gravitational stellar collapse been detected? Phys. Rev. Lett. 55, 1422–1425.
- Totani, T. and Sato, K. (1995) Spectrum of the relic neutrino background from past supernovae and cosmological models. Astropart. Phys. 3, 367–376.
- Totani, T., Sato, K. and Yoshii, Y. (1996) Spectrum of the supernova relic neutrino background and evolution of galaxies. Astrophys. J. 460, 303–312.
- Malaney, R.A. (1997) Evolution of the cosmic gas and the relic supernova neutrino background. Astropart. Phys. 7, 125–136.
- Hartmann, D.H. and Woosley, S.E. (1997) The cosmic supernova neutrino background. Astropart. Phys. 7, 137–146.
- 11) Kaplinghat, M., Steigman, G. and Walker, T.P. (2000) Supernova relic neutrino background. Phys. Rev. D **62**, 043001.
- 12) Ando, S., Sato, K. and Totani, T. (2003) Detectability of the supernova relic neutrinos and neutrino oscillation. Astropart. Phys. 18, 307– 318.
- Ando, S. and Sato, K. (2003) Supernova relic neutrinos and observational implications for neutrino oscillation. Phys. Lett. B 559, 113.
- 14) Fukugita, M. and Kawasaki, M. (2003) Constraints on the star formation rate from supernova relic neutrino observations. Mon. Not. Roy. Astron. Soc. 340, L7.
- 15) Strigari, L.E., Kaplinghat, M., Steigman, G. and Walker, T.P. (2004) The Supernova relic neutrino backgrounds at KamLAND and Super-Kamiokande. JCAP 0403, 007.

- 16) Iocco, F., Mangano, G., Miele, G., Raffelt, G.G. and Serpico, P.D. (2005) Diffuse cosmic neutrino background from Population III stars. Astropart. Phys. 23, 303–312.
- 17) Strigari, L.E., Beacom, J.F., Walker, T.P. and Zhang, P. (2005) The concordance cosmic star formation rate: Implications from and for the supernova neutrino and gamma ray backgrounds. JCAP 0504, 017.
- 18) Lunardini, C. (2006) The diffuse supernova neutrino flux, supernova rate and SN1987A. Astropart. Phys. 26, 190–201.
- Daigne, F., Olive, K.A., Sandick, P. and Vangioni, E. (2005) Neutrino signatures from the first stars. Phys. Rev. D 72, 103007.
- 20) Yuksel, H., Ando, S. and Beacom, J.F. (2006) Direct measurement of supernova neutrino emission parameters with a gadolinium-enhanced Super-Kamiokande detector. Phys. Rev. C 74, 015803.
- Horiuchi, S., Beacom, J.F. and Dwek, E. (2009) The diffuse supernova neutrino background is detectable in Super-Kamiokande. Phys. Rev. D 79, 083013.
- Lunardini, C. (2009) Diffuse neutrino flux from failed supernovae. Phys. Rev. Lett. 102, 231101.
- 23) Lien, A., Fields, B.D. and Beacom, J.F. (2010) Synoptic sky surveys and the diffuse supernova neutrino background: Removing astrophysical uncertainties and revealing invisible supernovae. Phys. Rev. D 81, 083001.
- 24) Keehn, J.G. and Lunardini, C. (2012) Neutrinos from failed supernovae at future water and liquid argon detectors. Phys. Rev. D 85, 043011.
- 25) Vissani, F. and Pagliaroli, G. (2011) The diffuse supernova neutrino background: Expectations and uncertainties derived from SN1987A. Astron. Astrophys. 528, L1.
- 26) Lunardini, C. and Tamborra, I. (2012) Diffuse supernova neutrinos: oscillation effects, stellar cooling and progenitor mass dependence. JCAP 1207, 012.
- 27) Nakazato, K. (2013) Imprint of explosion mechanism on supernova relic neutrinos. Phys. Rev. D 88, 083012.
- 28) Mathews, G.J., Hidaka, J., Kajino, T. and Suzuki, J. (2014) Supernova relic neutrinos and the supernova rate problem: Analysis of uncertainties and detectability of ONeMg and failed supernovae. Astrophys. J. 790, 115.
- Yuksel, H. and Kistler, M.D. (2015) The cosmic MeV neutrino background as a laboratory for black hole formation. Phys. Lett. B 751, 413–417.
- 30) Nakazato, K., Mochida, E., Niino, Y. and Suzuki, H. (2015) Spectrum of the supernova relic neutrino background and metallicity evolution of galaxies. Astrophys. J. 804, 75.
- 31) Hidaka, J., Kajino, T. and Mathews, G.J. (2016) Red-supergiant and supernova rate problems: Implication for the relic supernova neutrino spectrum. Astrophys. J. 827, 85.
- 32) Priya, A. and Lunardini, C. (2017) Diffuse neutrinos from luminous and dark supernovae: Prospects for

- upcoming detectors at the $\mathcal{O}(10)$ kt scale. JCAP 11, 031.
- 33) Horiuchi, S., Sumiyoshi, K., Nakamura, K., Fischer, T., Summa, A., Takiwaki, T. et al. (2018) Diffuse supernova neutrino background from extensive core-collapse simulations of 8-100M_☉ progenitors. Mon. Not. Roy. Astron. Soc. 475, 1363–1374.
- 34) Møller, K., Suliga, A.M., Tamborra, I. and Denton, P.B. (2018) Measuring the supernova unknowns at the next-generation neutrino telescopes through the diffuse neutrino background. JCAP 05, 066
- 35) Riya, V.R. (2020) Neutrinos from the cosmic noon: a probe of the cosmic star formation history. arXiv:2007.02951.
- 36) Kresse, D., Ertl, T. and Janka, H.-T. (2021) Stellar collapse diversity and the diffuse supernova neutrino background. Astrophys. J. 909, 169.
- 37) Ekanger, N., Horiuchi, S., Kotake, K. and Sumiyoshi, K. (2022) Impact of late-time neutrino emission on the diffuse supernova neutrino background. Phys. Rev. D 106, 043026.
- 38) Ziegler, J.J., Edwards, T.D.P., Suliga, A.M., Tamborra, I., Horiuchi, S., Ando, S. et al. (2022) Non-universal stellar initial mass functions: Large uncertainties in star formation rates at $z\approx 2-4$ and other astrophysical probes. Mon. Not. Roy. Astron. Soc. **517**, 2471–2484.
- 39) Ashida, Y. and Nakazato, K. (2022) Exploring the fate of stellar core collapse with supernova relic neutrinos. Astrophys. J. 937, 30.
- 40) Ashida, Y., Nakazato, K. and Tsujimoto, T. (2023) Diffuse neutrino flux based on the rates of corecollapse supernovae and black hole formation deduced from a novel galactic chemical evolution model. Astrophys. J. 953, 151.
- 41) Anandagoda, S., Hartmann, D.H., Fryer, C.L., Ajello, M., Desai, A., Hungerford, A.L. et al. (2023) Cosmic supernova neutrino and gammaray backgrounds in the MeV regime. Astrophys. J. 950, 29.
- 42) Ando, S. and Sato, K. (2004) Relic neutrino background from cosmological supernovae. New J. Phys. **6**, 170.
- 43) Beacom, J.F. (2010) The diffuse supernova neutrino background. Ann. Rev. Nucl. Part. Sci. **60**, 439–462.
- 44) Lunardini, C. (2016) Diffuse supernova neutrinos at underground laboratories. Astropart. Phys. 79, 49–77.
- 45) Mathews, G.J., Boccioli, L., Hidaka, J. and Kajino, T. (2020) Review of uncertainties in the cosmic supernova relic neutrino background. Mod. Phys. Lett. A 35, 2030011.
- 46) Kolb, E.W. and Turner, M.S. (1990) The Early Universe, CRC Press, Boca Raton.
- 47) Fogli, G.L., Lisi, E., Mirizzi, A. and Montanino, D. (2004) Three generation flavor transitions and decays of supernova relic neutrinos. Phys. Rev. D 70, 013001.
- 48) Planck Collaboration (2020) Planck 2018 results. VI. Cosmological parameters. Astron. Astrophys.

- **641**, A6, Erratum (2021) Astron. Astrophys. **652**, C4.
- 49) Cappellaro, E., Evans, R. and Turatto, M. (1999) A new determination of supernova rates and a comparison with indicators for galactic star formation. Astron. Astrophys. 351, 459.
- 50) Cappellaro, E., Riello, M., Altavilla, G., Botticella, M.T., Benetti, S., Clocchiatti, A. et al. (2005) Death rate of massive stars at redshift ~0.3. Astron. Astrophys. 430, 83.
- 51) Botticella, M.T., Riello, M., Cappellaro, E., Benetti, S., Altavilla, G., Pastorello, A. et al. (2008) Supernova rates from the Southern inTermediate Redshift ESO Supernova Search (STRESS). Astron. Astrophys. 479, 49–66.
- 52) Leaman, J., Li, W., Chornock, R. and Filippenko, A.V. (2011) Nearby supernova rates from the lick observatory supernova search. I. The methods and database. Mon. Not. Roy. Astron. Soc. 412, 1419.
- 53) Li, W., Leaman, J., Chornock, R., Filippenko, A.V., Poznanski, D., Ganeshalingam, M. et al. (2011) Nearby supernova rates from the Lick Observatory Supernova Search. II. The observed luminosity functions and fractions of supernovae in a complete sample. Mon. Not. Roy. Astron. Soc. 412, 1441.
- 54) Li, W., Chornock, R., Leaman, J., Filippenko, A.V., Poznanski, D., Wang, X. et al. (2011) Nearby supernova rates from the Lick Observatory Supernova Search. III. The rate-size Relation, and the rates as a function of Galaxy Hubble type and colour, Mon. Not. Roy. Astron. Soc. 412, 1473.
- 55) Ivezić, Ž., Kahn, S.M., Tyson, J.A., Abel, B., Acosta, E., Allsman, R. et al. (2019) LSST: from science drivers to reference design and anticipated data products. Astrophys. J. 873, 111.
- 56) Lien, A. and Fields, B.D. (2009) Cosmic corecollapse supernovae from upcoming sky surveys. JCAP 01, 047.
- 57) Mattila, S., Dahlen, T., Efstathiou, A., Kankare, E., Melinder, J., Alonso-Herrero, A. et al. (2012) Core-collapse supernovae missed by optical surveys. Astrophys. J. 756, 111.
- Mannucci, F., Della Valle, M. and Panagia, N. (2007) How many supernovae are we missing at high redshift? Mon. Not. Roy. Astron. Soc. 377, 1229–1235.
- 59) Horiuchi, S., Beacom, J.F., Kochanek, C.S., Prieto, J.L., Stanek, K.Z. and Thompson, T.A. (2011) The cosmic core-collapse supernova rate does not match the massive-star formation rate. Astrophys. J. 738, 154–169.
- 60) Lovegrove, E. and Woosley, S.E. (2013) Very Low Energy Supernovae from Neutrino Mass Loss. Astrophys. J. 769, 109.
- 61) Lovegrove, E., Woosley, S.E. and Zhang, W. (2017) Very low energy supernovae: Light curves and spectra of shock breakout. Astrophys. J. 845, 103.
- 62) Gerke, J.R., Kochanek, C.S. and Stanek, K.Z. (2015) The search for failed supernovae with the

- Large Binocular Telescope: First candidates. Mon. Not. Roy. Astron. Soc. **450**, 3289–3305.
- 63) Neustadt, J.M.M., Kochanek, C.S., Stanek, K.Z., Basinger, C.M., Jayasinghe, T., Garling, C.T. et al. (2021) The search for failed supernovae with the Large Binocular Telescope: a new candidate and the failed SN fraction with 11 yr of data. Mon. Not. Roy. Astron. Soc. 508, 516–528.
- 64) Byrne, R. and Fraser, M. (2022) Nothing to see here: failed supernovae are faint or rare. Mon. Not. Roy. Astron. Soc. 514, 1188–1205.
- 65) Horiuchi, S. and Beacom, J.F. (2010) Revealing Type Ia supernova physics with cosmic rates and nuclear gamma rays. Astrophys. J. 723, 329–341.
- 66) Salpeter, E.E. (1955) The luminosity function and stellar evolution. Astrophys. J. 121, 161–167.
- 67) Chabrier, G. (2003) Galactic stellar and substellar initial mass function. Publ. Astron. Soc. Pac. 115, 763–796.
- 68) Kroupa, P. (2001) On the variation of the initial mass function. Mon. Not. Roy. Astron. Soc. 322, 231.
- 69) Kennicutt, R.C., Jr. (1998) Star formation in galaxies along the Hubble sequence. Ann. Rev. Astron. Astrophys. 36, 189–231.
- 70) Yuksel, H., Kistler, M.D., Beacom, J.F. and Hopkins, A.M. (2008) Revealing the high-redshift star formation rate with gamma-ray bursts. Astrophys. J. Lett. 683, L5–L8.
- Madau, P. and Dickinson, M. (2014) Cosmic star formation history. Ann. Rev. Astron. Astrophys. 52, 415–486.
- 72) Audcent-Ross, F.M., Meurer, G.R., Wong, O.I., Zheng, Z., Hanish, D., Zwaan, M.A. et al. (2018) Near-identical star formation rate densities from $H\alpha$ and FUV at redshift zero. Mon. Not. Roy. Astron. Soc. **480**, 119–133.
- 73) Kochanek, C.S., Beacom, J.F., Kistler, M.D., Prieto, J.L., Stanek, K.Z., Thompson, T.A. et al. (2008) A survey about nothing: Monitoring a million supergiants for failed supernovae. Astrophys. J. 684, 1336–1342.
- 74) Adams, S.M., Kochanek, C.S., Gerke, J.R., Stanek, K.Z. and Dai, X. (2017) The search for failed supernovae with the Large Binocular Telescope: confirmation of a disappearing star. Mon. Not. Roy. Astron. Soc. 468, 4968–4981.
- 75) Adams, S.M., Kochanek, C.S., Gerke, J.R. and Stanek, K.Z. (2017) The search for failed supernovae with the Large Binocular Telescope: constraints from 7 yr of data. Mon. Not. Roy. Astron. Soc. 469, 1445–1455.
- 76) Basinger, C.M., Kochanek, C.S., Adams, S.M., Dai, X. and Stanek, K.Z. (2021) The search for failed supernovae with the Large Binocular Telescope: N6946-BH1, still no star. Mon. Not. Roy. Astron. Soc. 508, 1156-1164.
- 77) Graur, O., Bianco, F.B. and Modjaz, M. (2015) A unified explanation for the supernova rate-galaxy mass dependence based on supernovae detected in Sloan galaxy spectra. Mon. Not. Roy. Astron. Soc. 450, 905–925.

- 78) Woosley, S.E., Heger, A. and Weaver, T.A. (2002) The evolution and explosion of massive stars. Rev. Mod. Phys. 74, 1015–1071.
- 79) O'Connor, E. and Ott, C.D. (2011) Black Hole formation in failing core-collapse supernovae. Astrophys. J. 730, 70.
- 80) Ugliano, M., Janka, H.T., Marek, A. and Arcones, A. (2012) Progenitor-explosion connection and remnant birth masses for neutrino-driven supernovae of iron-core progenitors. Astrophys. J. 757, 69.
- 81) Pejcha, O. and Thompson, T.A. (2015) The landscape of the neutrino mechanism of core-collapse supernovae: Neutron star and black hole mass functions, explosion energies and nickel yields. Astrophys. J. 801, 90.
- 82) Nakamura, K., Takiwaki, T., Kuroda, T. and Kotake, K. (2015) Systematic features of axisymmetric neutrino-driven core-collapse supernova models in multiple progenitors. Publ. Astron. Soc. Jpn. 67, 107.
- 83) Sukhbold, T., Ertl, T., Woosley, S.E., Brown, J.M. and Janka, H.T. (2016) Core-collapse supernovae from 9 to 120 solar masses based on neutrino-powered explosions. Astrophys. J. 821, 38.
- 84) Tsang, B.T.H., Vartanyan, D. and Burrows, A. (2022) Applications of machine learning to predicting core-collapse supernova explosion outcomes. Astrophys. J. Lett. 937, L15.
- 85) Sana, H., de Mink, S.E., de Koter, A., Langer, N., Evans, C.J., Gieles, M. et al. (2012) Binary interaction dominates the evolution of massive stars. Science 337, 444.
- 86) Horiuchi, S., Kinugawa, T., Takiwaki, T., Takahashi, K. and Kotake, K. (2021) Impact of binary interactions on the diffuse supernova neutrino background. Phys. Rev. D 103, 043003.
- 87) Kotake, K., Sato, K. and Takahashi, K. (2006) Explosion mechanism, neutrino burst, and gravitational wave in core-collapse supernovae. Rept. Prog. Phys. 69, 971–1144.
- 88) Mirizzi, A., Tamborra, I., Janka, H.-T., Saviano, N., Scholberg, K., Bollig, R. et al. (2016) Supernova neutrinos: Production, oscillations and detection. Riv. Nuovo Cim. 39, 1.
- 89) Janka, H.T. (2017) Neutrino emission from supernovae. In Handbook of Supernovae (eds. Alsabti, A. and Murdin, P.). Springer, Cham, pp. 1575– 1604.
- 90) Burrows, A. and Vartanyan, D. (2021) Corecollapse supernova explosion theory. Nature 589, 29–39.
- 91) Bollig, R., Yadav, N., Kresse, D., Janka, H.T., Müller, B. and Heger, A. (2021) Self-consistent 3D supernova models from -7 minutes to +7s: A 1-bethe explosion of a $\sim 19\,M_{\odot}$ Progenitor. Astrophys. J. **915**, 28.
- 92) O'Connor, E., Bollig, R., Burrows, A., Couch, S., Fischer, T., Janka, H.-T. et al. (2018) Global comparison of core-collapse supernova simulations in spherical symmetry. J. Phys. G 45, 104001.
- 93) Baxter, A.L., BenZvi, S., Jaimes, J.C., Coleiro, A.,

- Molla, M.C., Dornic, D. et al. (2021) Snewpy: A data pipeline from supernova simulations to neutrino signals. J. Open Source Software 6, 3772.
- 94) The SNEWS Collaboration (2022) SNEWPY: A data pipeline from supernova simulations to neutrino signals. Astrophys. J. **925**, 107.
- 95) Nakazato, K., Sumiyoshi, K., Suzuki, H., Totani, T., Umeda, H. and Yamada, S. (2013) Supernova neutrino light curves and spectra for various progenitor stars: From core collapse to protoneutron star cooling. Astrophys. J. Suppl. 205, 2.
- 96) Nagakura, H., Burrows, A. and Vartanyan, D. (2021) Supernova neutrino signals based on long-term axisymmetric simulations. Mon. Not. Roy. Astron. Soc. 506, 1462–1479.
- 97) Kuroda, T. (2021) Impact of a magnetic field on neutrino-matter interactions in core-collapse supernovae. Astrophys. J. 906, 128.
- 98) Tamborra, I., Raffelt, G., Hanke, F., Janka, H.-T. and Mueller, B. (2014) Neutrino emission characteristics and detection opportunities based on three-dimensional supernova simulations. Phys. Rev. D 90, 045032.
- 99) Particle Data Group (2022) Review of particle physics. PTEP 2022, 083C01.
- 100) Raaijmakers, G., Greif, S.K., Hebeler, K., Hinderer, T., Nissanke, S., Schwenk, A. et al. (2021) Constraints on the dense matter equation of state and neutron star properties from NICER's mass-radius estimate of PSR J0740+6620 and multimessenger observations. Astrophys. J. Lett. 918, L29
- 101) Yuksel, H. and Beacom, J.F. (2007) Neutrino spectrum from SN 1987A and from cosmic supernovae. Phys. Rev. D 76, 083007.
- 102) Shen, H., Toki, H., Oyamatsu, K. and Sumiyoshi, K. (1998) Relativistic equation of state of nuclear matter for supernova and neutron star. Nucl. Phys. A. 637, 435–450.
- 103) Tabrizi, Z. and Horiuchi, S. (2021) Flavor triangle of the diffuse supernova neutrino background. JCAP 05, 011.
- 104) Suliga, A.M., Beacom, J.F. and Tamborra, I. (2022) Towards probing the diffuse supernova neutrino background in all flavors. Phys. Rev. D 105, 043008.
- 105) Baum, S., Stengel, P., Abe, N., Acevedo, J.F., Araujo, G.R., Asahara, Y. et al. (2023) Mineral detection of neutrinos and dark matter. A whitepaper. Phys. Dark Univ. 41, 101245.
- 106) Baum, S., Capozzi, F. and Horiuchi, S. (2022) Rocks, water, and noble liquids: Unfolding the flavor contents of supernova neutrinos. Phys. Rev. D 106, 123008.
- 107) Baum, S., Edwards, T.D.P., Kavanagh, B.J., Stengel, P., Drukier, A.K., Freese, K. et al. (2020) Paleodetectors for Galactic supernova neutrinos. Phys. Rev. D 101, 103017.
- 108) Ando, S. (2003) Decaying neutrinos and implications from the supernova relic neutrino observation. Phys. Lett. B 570, 11.
- 109) De Gouvêa, A., Martinez-Soler, I., Perez-Gonzalez,

- Y.F. and Sen, M. (2020) Fundamental physics with the diffuse supernova background neutrinos. Phys. Rev. D **102**, 123012.
- 110) Jeong, Y.S., Palomares-Ruiz, S., Reno, M.H. and Sarcevic, I. (2018) Probing secret interactions of eV-scale sterile neutrinos with the diffuse supernova neutrino background. JCAP 06, 019.
- 111) Barranco, J., Bernal, A. and Delepine, D. (2018) Diffuse neutrino supernova background as a cosmological test. J. Phys. G 45, 055201.
- 112) Super-Kamiokande Collaboration (2021) Diffuse supernova neutrino background search at Super-Kamiokande. Phys. Rev. D 104, 122002.
- 113) Strumia, A. and Vissani, F. (2003) Precise quasie-lastic neutrino/nucleon cross-section. Phys. Lett. B **564**, 42–54.
- 114) Vogel, P. and Beacom, J.F. (1999) Angular distribution of neutron inverse beta decay, $\bar{\nu}_e + \overrightarrow{p}e^+ + n$. Phys. Rev. D **60**, 053003.
- 115) Zhang, W., Beier, E.W., Feldscher, L., Frank, E.D., Frati, W., Kim, S.B. et al. (1988) Experimental limit on the flux of relic antineutrinos from past supernovae. Phys. Rev. Lett. 61, 385–388.
- 116) Aglietta, M., Antonioli, P., Badino, G., Bologna, G., Castagnoli, C. and Castellina, A. (1992) Limits on low-energy neutrino fluxes with the mont blanc liquid scintillator detector. Astropart. Phys. 1, 1-9.
- 117) Super-Kamiokande Collaboration (1998) Evidence for oscillation of atmospheric neutrinos. Phys. Rev. Lett. 81, 1562–1567.
- 118) Super-Kamiokande Collaboration (2003) Search for supernova relic neutrinos at Super-Kamiokande. Phys. Rev. Lett. 90, 061101.
- 119) Super-Kamiokande Collaboration (2012) Supernova relic neutrino search at Super-Kamiokande. Phys. Rev. D 85, 052007.
- 120) Nishino, H., Awai, K., Hayato, Y., Kaneyuki, K., Nakayama, S., Okumura, K. et al. (2007) The new front-end electronics for the Super-Kamiokande experiment. In 2007 IEEE Nuclear Science Symposium Conference Record, Honolulu, HI, USA, 2007. IEEE, Vol. 1, pp. 127–132.
- 121) Super-Kamiokande Collaboration (2015) Supernova relic neutrino search with neutron tagging at Super-Kamiokande-IV. Astropart. Phys. 60, 41– 46.
- 122) SNO Collaboration (2002) Direct evidence for neutrino flavor transformation from neutral-current interactions in the sudbury neutrino observatory. Phys. Rev. Lett. 89, 011301.
- 123) SNO Collaboration (2004) Electron antineutrino search at the sudbury neutrino observatory. Phys. Rev. D **70**, 093014.
- 124) Aharmim, B., Ahmed, S.N., Anthony, A.E., Beier, E.W., Bellerive, A., Bergevin, M. et al. (2006) A search for neutrinos from the solar hep reaction and the diffuse supernova neutrino background with the sudbury neutrino observatory. Astrophys. J. 653, 1545.
- 125) Gando, A., Gando, Y., Ichimura, K., Ikeda, H., Inoue, K., Kibe, Y. et al. (2012) Search for

- extraterrestrial antineutrino sources with the KamLAND detector. Astrophys. J. **745**, 193.
- 126) KamLAND Collaboration (2022) Limits on astrophysical antineutrinos with the KamLAND experiment. Astrophys. J. 925, 14.
- 127) Agostini, M., Altenmüller, K., Appel, S., Atroshchenko, V., Bagdasarian, Z., Basilico, D. et al. (2021) Search for low-energy neutrinos from astrophysical sources with Borexino. Astropart. Phys. 125, 102509.
- 128) Super-Kamiokande Collaboration (2023) Search for astrophysical electron antineutrinos in Super-Kamiokande with 0.01% gadolinium-loaded water. Astrophys. J. Lett. **951**, L27.
- 129) Ankowski, A.M., Benhar, O., Mori, T., Yamaguchi, R. and Sakuda, M. (2012) Analysis of γ-ray production in neutral-current neutrino-oxygen interactions at energies above 200 mev. Phys. Rev. Lett. 108, 052505.
- 130) Kim, K. and Cheoun, M.-K. (2009) Roles of one-step process on neutrino scattering off 12c. Phys. Lett. B **679**, 330–333.
- 131) Baldoncini, M., Callegari, I., Fiorentini, G., Mantovani, F., Ricci, B., Strati, V. et al. (2015) Reference worldwide model for antineutrinos from

- reactors. Phys. Rev. D 91, 065002.
- 132) Beacom, J.F. and Vagins, M.R. (2004) GADZOOKS! Anti-neutrino spectroscopy with large water Cherenkov detectors. Phys. Rev. Lett. 93, 171101.
- 133) Marti, L.L., Ikeda, M., Kato, Y., Kishimoto, Y., Nakahata, M., Nakajima, Y. et al. (2020) Evaluation of gadolinium's action on water cherenkov detector systems with egads. Nucl. Instrum. Methods Phys. Res. A 959, 163549.
- 134) Abe, K., Bronner, C., Hayato, Y., Hiraide, K., Ikeda, M., Imaizumi, S. et al. (2022) First gadolinium loading to Super-Kamiokande. Nucl. Instrum. Methods Phys. Res. A 1027, 166248.
- 135) Abusleme, A., Adam, T., Ahmad, S., Ahmed, R., Aiello, S., Akram, M. et al. (2022) Prospects for detecting the diffuse supernova neutrino background with juno. J. Cosmol. Astropart. Phys. 2022, 033.
- Hyper-Kamiokande Proto-Collaboration (2018) Hyper-Kamiokande design report. arXiv:1805.04163.

(Received June 29, 2023; accepted Sep. 14, 2023)